Smart Structures and Systems, *Vol. 32, No. 5 (2023) 297-308*
https://doi.org/10.12989/sss.2023.32.5.297

Dynamic deflection monitoring method for long-span cable-stayed bridge based on bi-directional long short-term memory neural network

Yi-Fan Li [1a], Wen-Yu He*[1], Wei-Xin Ren [2b], Gang Liu [3] and Hai-Peng Sun [3]

[1] *Department of Civil Engineering, Hefei University of Technology, Hefei, Anhui 230009, China*
[2] *College of Civil and Transportation Engineering, Shenzhen University, Shenzhen, Guangdong 518061, China*
[3] *China Design Group, Nanjing, Jiangsu 210000, China*

(*Received June 3, 2022, Revise October 8, 2023, Accepted October 20, 2023*)

Abstract. Dynamic deflection is important for evaluating the performance of a long-span cable-stayed bridge, and its continuous measurement is still cumbersome. This study proposes a dynamic deflection monitoring method for cable-stayed bridge based on Bi-directional Long Short-term Memory (BiLSTM) neural network taking advantages of the characteristics of spatial variation of cable acceleration response (CAR) and main girder deflection response (MGDR). Firstly, the relationship between the spatial and temporal variation of the CAR and the MGDR is described based on the geometric deformation of the bridge. Then a data-driven relational model based on BiLSTM neural network is established using CAR and MGDR data, and it is further used to monitor the MGDR via measuring the CAR. Finally, numerical simulations and field test are conducted to verify the proposed method. The root mean squared error (RMSE) of the numerical simulations are less than 4 while the RMSE of the field test is 1.5782, which indicate that it provides a cost-effective and convenient method for real-time deflection monitoring of cable-stayed bridges.

Keywords: BiLSTM; cable acceleration; cable-stayed bridge; dynamic deflection

1. Introduction

Cable-stayed bridges are widely used due to their elegant appearance and long spanning capability. As the dynamic deflection is meaningful in reflecting the bridge health state, its real-time monitoring is essential for the cable-stayed bridges (Ni *et al*. 2019, 2020). Various methods for measuring bridge deflection have been developed in recent years. Instruments such as theodolite, level, and total station were widely used to measure bridge deflection in the early stage (Beshr and Kaloop 2013). However, these traditional measurement methods cannot achieve continuous and automatic measurement due to the need for constantly changing the monitoring positions and reference points, and the measurement accuracy is seriously affected by climatic factors.

At present, there are four main type methods to monitor deflection directly, specific as: (1) Displacement sensors, such as laser vibrometer and linear variable differential vibrometer (Nguyen *et al*. 2016, Shin *et al*. 2016, Li *et al*. 2020), which need to be installed on a fixed reference position, thus it is difficult to implement for actual long-span bridges; (2) Visual-based methods, such as cameras (Avsar *et al*. 2014, Khuc and Catbas 2017, Xu *et al*. 2018, Yu *et al*. 2021, Lee and Koh 2021) and multi-UAS (Zhuge *et al*. 2022), which are highly influenced by weather and vision situations; (3) GPS (Gaxiola-Camacho *et al*. 2017, Yi *et al*. 2017, Stiros 2021), which has the disadvantages of low sampling rate, low resolution and high cost; (4) Connecting tube (Zhou *et al*. 2021), which can only measure the dynamic deflection with low sampling rate.

To overcome the above-mentioned drawbacks of direct methods, various indirect methods have been developed. Park *et al*. (2005) proposed a method for estimating the initial velocity using bridge acceleration response and then reconstructing the deflection response. Pendharkar *et al*. (2010) developed a neural network for the continues composite beams to predict the in elastic mid-span deflections. Tadesse *et al*. (2012) developed neural networks for predicting the deflection of steel-concrete composite bridges under service loads. Ma *et al*. (2014) recovering the structural displacements from acceleration measurements. Huang *et al*. (2017) used persistent scatterer interferometry to monitor the dynamic deflection of the Dashengguan Yangtze River high-speed railroad bridge. Wang *et al*. (2021) proposed an indirect strain based dynamic displacement reconstruction methodology for high-speed railway box girders. He *et al*. (2022) estimated the moving load induced deflection based on the fusion of acceleration and strain response data. However, such methods are valid for small span bridges as a large number of sensors are required to be installed for long-span bridges in order to provide accurate monitoring results.

Therefore, attention has been further paid to indirect deflection measurement for long-span bridges, especially cable-stayed bridges. Huang *et al*. (2018) established the

*Corresponding author, Ph.D., Professor,
E-mail: wyhe@hfut.edu.cn
[a] Ph.D. Student
[b] Ph.D., Professor

ISSN: 1738-1584 (Print), 1738-1991 (Online)

relationship equation between the cable force and the displacement of the anchorage point between the cable and the main girder. And then the displacement of the anchorage point was monitored by the time-varying cable force obtained by cable acceleration response and the relationship equation. However, only the deflection of the anchorage point corresponding to the measured cable could be monitored via this approach. A large number of acceleration sensors should be installed when the deflections of many anchorage points were required.

In addition, with the development of deep learning, neural networks have been extensively used for dynamic response reconstruction in the field of structural health monitoring. Fan *et al*. (2019) recovered the lost data of health monitoring system based on convolution neural network. Further, this methodology was refined by using residual convolutional networks to remove noise from health monitoring signals for accurate structural modal identification (Fan *et al*. 2020), and a generative adversarial network based method for reconstructing the structural dynamic response was proposed accordingly (Fan *et al*. 2021). Meanwhile, deep learning has been also proven invaluable in the health monitoring of cable-stayed bridge. Tian *et al*. (2021) used bi-directional long short-term memory (BiLSTM) neural network to describe the relationship between cable force and bridge deflection based on long-term monitoring data, and then employed the measured deflection to monitor the cable force. However, it is normally difficult and expensive to continuously monitor the deflection of actual bridges. Besides, if this relationship model was used to monitor the deflection through cable force, unnecessary errors would be introduced during the estimation process from cable acceleration to cable forces.

In view of this, this paper proposes a main girder deflection response (MGDR) monitoring method directly using cable acceleration response (CAR). As the relationship between CAR and MGDR is difficult to represent by explicit expression, the fitting ability of BiLSTM neural network is utilized to model the relationship between CAR and MGDR in terms of spatial and temporal variation. The indirect monitoring method for MGDR through measuring the CAR is then proposed accordingly. Numerical simulations and field tests are conducted to verify the feasibility and effectiveness of the proposed method. The root mean squared error (RMSE) of numerical simulations are less than 4, while the RMSE of the field test is 1.5782.

2. Methodology

2.1 The geometric deformation relationship between the girder and cable

Assuming that the stiffness of the bridge tower is infinite, then the cable force change is mainly caused by girder deflection. The geometric deformation relationship without considering the effect of the longitudinal motion of the girder on its deflection is shown in Fig. 1 (Huang *et al*. 2018), in which the red solid line and blue dashed line denote the geometric before and after deformation respectively. The following equation can be obtained

$$\delta = \frac{\gamma}{\sin\alpha} = \frac{L}{EA\sin\alpha}\Delta T \tag{1}$$

in which δ is the anchorage deflection between the cable and the main girder; γ is the cable elongation caused by the anchorage deflection; α is the angle between the cable and the main girder; ΔT is the cable force change caused by the anchorage deflection; E, $A$and L are the elasticity modulus, cross-sectional area, and length of the cable, respectively.

According to Eq. (1), the cable tension is linearly related to the anchorage deflection. Besides, the relationship between cable frequency and cable force can be expressed as (Irvine 1981)

$$T = 4ml^2\left(\frac{f_n}{n}\right)^2 \tag{2}$$

where f_n is the n^{th} order frequency; T, m and l are the cable force, the mass of per unit length of cable and cable length, respectively.

It can be concluded from Eq. (2) that the frequency changes with the variation of the real-time cable force, and the frequency change will significantly influence the signal characteristics. For example, when the MGDR change

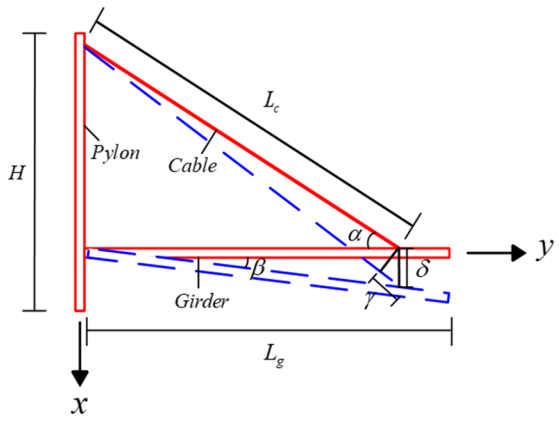

Fig. 1 Deflection of the anchorage

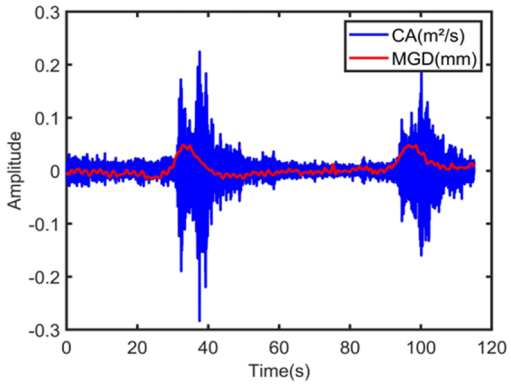

Fig. 2 Relationship between CAR and MGDR

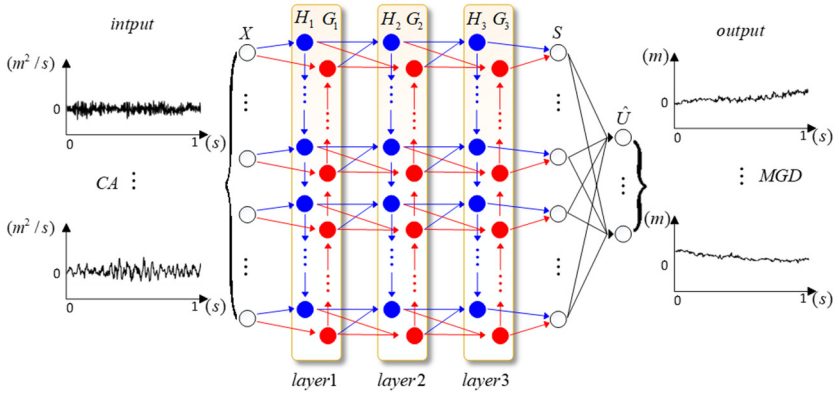

Fig. 3 Architecture of the BiLSTM model

causes a sudden change (inflection point) in the cable force, the CAR response will oscillate violently, as shown in Fig. 2. Thus, it is possible to develop a data-driven model for monitoring MGDR through CAR by taking advantages of the characteristics of spatial and temporal variation of CAR and MGDR.

2.2 Architecture of the BiLSTM model

Developing a detail finite element model for response analysis is challenging due to the spatial and temporal distribution of various loads on complex bridges. Therefore, a data-driven neural network technique is employed to represent the relationship between CAR and MGDR based on BiLSTM. As shown in Fig. 3, the BiLSTM combines forward and backward LSTM, which consists of inputs $\boldsymbol{X}_t$, forward transmission hidden states $\boldsymbol{H}_t$, backward transmission hidden state $\boldsymbol{G}_t$, intermediate state $\boldsymbol{S}_t$, and outputs $\hat{U}_t$. CAR and MGDR are set as inputs and target outputs in this study, respectively. The input and target outputs are represented as

$$X_t = [X_t^1, X_t^2, \ldots, X_t^M] \tag{3a}$$

$$\hat{U}_t = [\hat{U}_t^1, \hat{U}_t^2, \ldots, \hat{U}_t^N] \tag{3b}$$

where M and N denote the number of input (CAR) channels and output (MGDR) channels, respectively. Noted that X_t and $\hat{U}_t$ are the input and output data after preprocessing, and the detailed preprocessing procedure will be described in Section 3.

And LSTM is the basic cell of BiLSTM, which is composed of immediate input gate x_t, cell state C_t, temporary cell state $\tilde{C}_t$, hidden state h_t, forgetting gate f_t, memory gate i_t, and output gate o_t. The computation process of LSTM is shown in Fig. 4. During network training, the useful information for subsequent moments of computation is passed while the useless information is discarded through forgetting the old information and remembering the new information in the cell state, and the output at each time step is provide by hidden state. The value of forgetting gate f_t in the LSTM cell can be calculated as

$$f_t = \sigma(W_f \cdot [h_{t-1}, x_t] + b_f) \tag{4}$$

where W_f and b_f denote the weight and bias of forgetting gate f_t, respectively; $[h_{t-1}, x_t]$ denote the vector spliced by h_{t-1} and x_t; $\sigma(\cdot)$is the sigmoid activation function. The computation method of input gate x_t and output gate o_t are the same as forgetting gate f_t except the values of the parameters.

The cell state C_t consists of two parts: one is related to the multiplication of the previous cell state C_{t-1} and the forgotten gate f_t, and the other is related to the temporary cell state $\tilde{C}_t$. It can be computed by Eq. (5)

$$\tilde{C}_t = tanh(W_c[h_{t-1}, x_t] + b_c) C_t = f_t \cdot C_{t-1} + i_t \cdot \tilde{C}_t \tag{5}$$

Then, the hidden state h_t is calculated by the current cell state C_t and the output gate o_t as

$$h_t = o_t \bullet tanh(C_t) \tag{6}$$

where $\bullet$ denotes the point multiplication of two vectors.

The loss value computed by the loss function L is used to update the network model by error back propagation from outputs to inputs. The model parameters are iteratively optimized by the backpropagation algorithm based on gradient descent. Taking ω as general parameter to be optimized and η as learning rate, the parameter optimization process is carried out by Adam optimizer (Kingma and Ba 2021)

$$\omega_k = \omega_{k-1} - \eta \times Adam(\frac{\partial L(k-1)}{\partial \omega}) \tag{7}$$

where L is loss function, as

$$L = \frac{1}{mn} \sum_{i=1}^{m} \sum_{t=1}^{n} [(U_t^i - \hat{U}_t^i)^2 \times |U_t^i|] \tag{8}$$

where U_t^i and $\hat{U}_t^i$ denote the measured output and predicted output of i -th channel at time t, respectively.

2.3 The BiLSTM model for bridge CAR and MGDR

Considering the spatial and temporal variation effects between CAR and MGDR, the BiLSTM neural network is used to establish a data-driven model for the sequence relationship between CAR and MGDR. The parameters H_t, G_t, S_t of the same layer are shared for each time step. If only the information corresponding to the time moment is taken as input, the available relevant information will be reduced, which will lead to a large prediction error. Therefore, the input length is set to be greater than the output length in this study. Three interconnected hidden layers are designed considering that a single hidden layer is unable to simulate a complex system.

The MGDR produces significant peaks when the bridge is subjected to vehicle loads. Therefore, an effective weighting strategy is introduced in order to fit these peaks more accurately. Specifically, the $\left|U_t^i\right|$ is used as a weight which is multiplied with $(U_t^i - \hat{U}_t^i)^2$at each discrete time point t. This approach ensures that the results are more focused on the characteristics of the peaks described above. As a result, the fusion of $\left|U_t^i\right|$ and $(U_t^i - \hat{U}_t^i)^2$ improves the accuracy of the peak fitting while downplaying the effect of fluctuations around the zero point, thus building a more robust analytical framework for monitoring the MGDR under vehicle loading. Consequently, the fusion of $\left|U_t^i\right|$ and $(U_t^i - \hat{U}_t^i)^2$ not only augments the precision of peak fitting, but also attenuates the perturbations in proximity to the zero.

2.4 Deflection monitoring procedure

To overcome the limitations of existing methods, a new method for monitoring the cable-stayed bridge deflection using the CAR response is developed based on the BiLSTM model. And the new method consists of five steps:

Step 1: An acceleration sensor is installed at any position of the cable and a displacement sensor is installed at the position of the main girder of the cable-stayed bridge to be monitored. The CAR and MGDR response are collected synchronously.

Step 2: The BiLSTM neural network as introduced in Section 2.2 is established and the acquired signals are pre-processed. The specific pre-process will be described in Section 3.

Step 3: The CAR in the training set is used as model input. The output results and measured MGDR are used to calculate the loss function for updating the network. When the loss function remains stable, the network updating is stopped and the trained model is preserved.

Step 4: The CAR in the test set is fed into the trained model, and the final output is data-reduced by inverse transformation according to the data pre-processing procedure described in Section 3. Reasonable hyperparameters are determined by testing. The model is used as the final monitoring model until the output of the network agrees well with the monitoring results.

Step 5: Real-time monitoring of MGDR is achieved by inputting the monitored CAR into the trained model and data reconstruction of the corresponding outputs.

In summary, a model established by a small amount of CAR and MGDR data can be used to obtain the real-time deflection at certain locations of the cable-stayed bridge via the CAR. Therefore, the MGDR can be monitored by substituting the CARs that are already automatically monitored via the health monitoring system into the trained model. Compared with traditional methods, the proposed provides a more economical and convenient way to measure the real-time deflection.

3. Data pre-processing

3.1 Data normalization

Normalization is essential in data pre-processing when high variation exist in dataset features. The purpose of data normalization is to make the features have the same metric scale. Data that are not normalized may flatten in the final result due to the activation functions $\sigma(\cdot)$and $tanh(\cdot)$. Thus, the following normalization method is used in this study.

$$X_t^i = \frac{\tilde{X}_t^i}{max(\tilde{X}_l^i | l = 1 \dots k)}, i = 1 \dots M \tag{9a}$$

$$U_t^j = \frac{\tilde{U}_t^j}{max(\tilde{U}_l^j | l = 1 \dots k)}, j = 1 \dots N \tag{9b}$$

where $\tilde{X}_t^i$ and $\tilde{U}_t^j$ denote the original CAR data and MGDR data at time t, respectively; X_t^i and U_t^j denote the corresponding normalized data; l denote the number of sampling points; M and N are the number of data points of the CARs and MGDRs, respectively; i, j and l are the subscripts and superscripts, respectively.

Compared with the traditional normalization of data to the interval [0, 1], this method normalizes X_t^i and U_t^j to the interval [-1, 1], which is more suitable for function$tanh(\cdot)$. Finally, the results are converted to real scales by the corresponding normalization factors to obtain the actual response.

3.2 Data conversion

The data needs to be converted into a 3D torch according to the input format of BiLSTM. Generally speaking, the responses are often sampled at high sampling frequency for CAR and low sampling frequency for MGDR, i.e., the CAR and MGDR are not in one-to-one correspondence in time sequence, and it is necessary to divide the measured data into the format of $[batch\_size, seq\_len, input\_size]$ according to the sampling frequency, where $batch\_size$ denotes the data set size of each batch of input network which is determined by experiment; seq_len denotes the time step length; $input\_size$ denotes the input sequence data length. The data tensor is generated using transformed dataset in Section 3.1, and the data set is then divided into training set and test set.

4. Implementation details

The proposed BiLSTM model is trained on Pytorch (Paszke *et al*. 2019) which is a deep learning framework developed by Facebook. Pytorch provides various tensor operations and allows gradient computation through automatic derivation that facilitating the construction of various dynamic neural networks. Gradient-based Adam Optimizer is used for network parameter updating. The numerical experiments are carried out on a computer equipped with Intel Core i7-12700K CPU (with 16 GB RAM) and NVIDIA RTX 2070 GPU (with 8 GB RAM). The input dimension of the BiLSTM model is equal to the sampling frequency of CAR, while the output dimension is equal to the sampling frequency of MGDR. In this paper, the input dimension, output dimension, and hidden state dimension are set to be 1024, 60, and 128, respectively. The batch size and the number of iterations are set to be 16 and 2000, respectively. The initial learning rate is set to be 0.01 and decrease exponentially with the epoch.

5. Numerical verification

A numerical example of a cable-stayed bridge with a total length of 104 m is shown in Fig. 5. The cable-stayed bridge is a floating system, with the main girder supported by fixed bearings on the left pier and longitudinal movable bearings on the right pier, with no vertical supports between the main girder and the tower. The cables are numbered C1 ~ C14 from West to East (Fig. 5). The finite element model (FEM) of the cable-stayed bridge is established using ANSYS (Ansys Inc. 2014), in which the tower and main girder are simulated by Beam 188 element, and the cable is simulated by Link 10 element. The main parameters of the bridge are listed in Table 1. The MGDR of the monitoring point is calculated directly by the cable-stayed bridge FEM(BFEM), and then the displacement at the anchorage of the cables is extracted accordingly. Finally, the cable FEMs (CFEM) are established for each cable, and the displacements at the anchorage are applied on the cable FEMs as the vertical displacement excitation to extract the CAR responses. For simplicity, only the moving vehicles are considered as the external dynamic loads in the numerical study.

The basic procedures of the numerical verification are: (1) Obtaining the CAR and MGDR from the CFEM and BFEM, respectively. (2) Developing and training the BiLSTM neural network model using the CAR and MGDR. (3) Substituting the untrained CAR into the trained network to obtain the output results. (4) Estimating the real MGDR by anti-normalizing the output of the model.

5.1 Monitoring of MGDR induced by single vehicle

Fig. 5 shows the five CAR monitoring points (Point C1-C5) and four deflection monitoring points (Point M1-M4) on the cable-stayed bridge. Shock excitation is first applied on the midspan to make bridge vibrate freely, and then a single vehicle load with random mass and velocity is assumed acceleration response time histories of C1 and C4, respectively. Figs. 6(c)-(d) display the main girder deflection time histories of point M2 and M4, respectively. Further the CAR and MGDR responses obtained by the FEM are substituted into the BiLSTM neural network for training. In this part, three groups of vehicles with different velocities and masses are selected. The two vehicles included in each group pass the cable-stayed bridge at different times, and the values of these velocity and mass combinations do not appear in the training set. In these

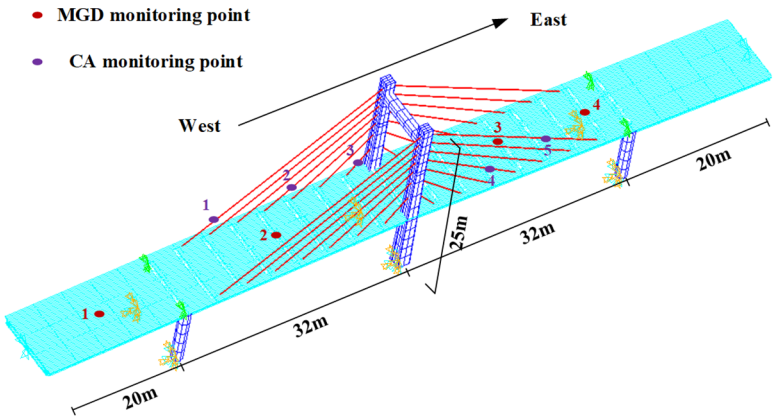

Fig. 5 The numerical cable-stayed bridge

Table 1 Parameters of the numerical cable-stayed bridge

	Young's modulus (GPa)	Density (kg/m^3)	Cross-sectional area (m^2)	Inertia moment (m^4)	Hight (m)
Cable	200	8500	3.31665e-3	9.35e-7	\
Girder	36	2600	5.330	49.050	8.5
Pylon	36	2600	2.762	0.686	25.0

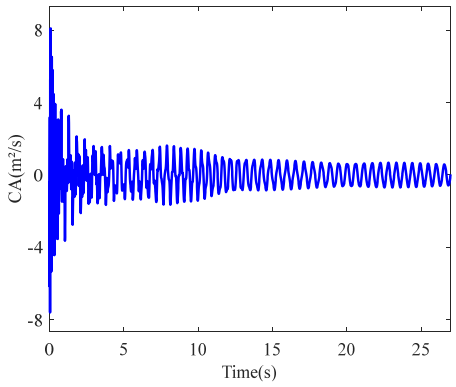

(a) The acceleration of C1

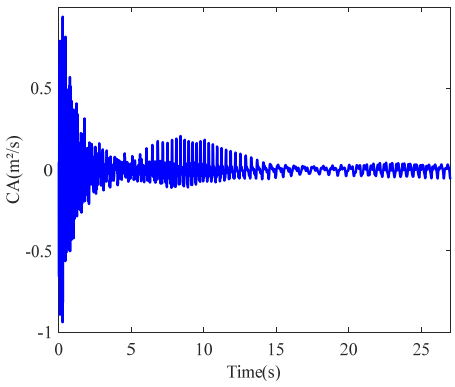

(b) The acceleration of C11

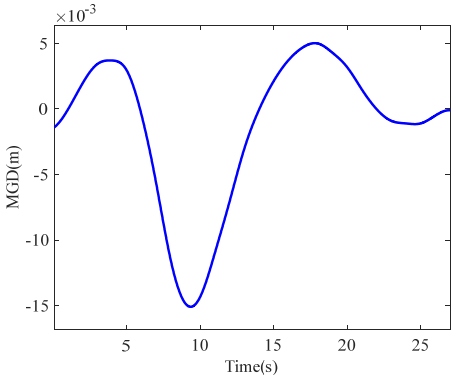

(c) The deflection of M2

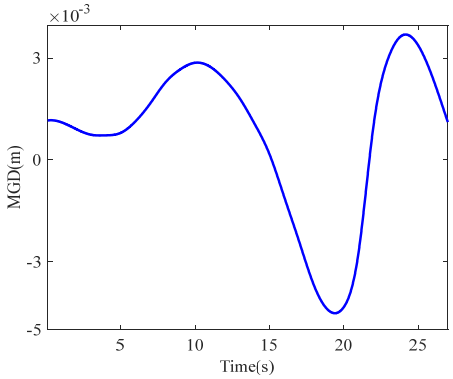

(d) The deflection of M4

Fig. 6 Response of numerical cable-stayed bridge induced by single moving vehicle

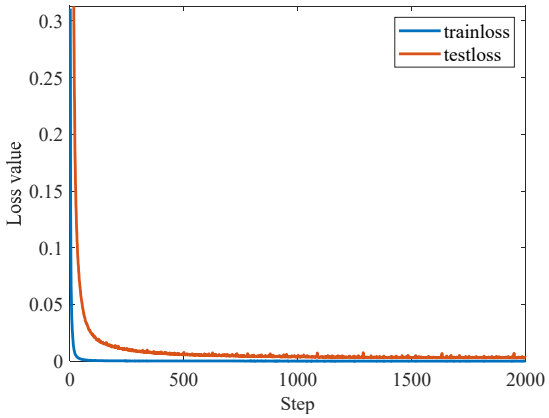

Fig. 7 The Loss curves for the monitoring model of MGDR induced by single vehicle

groups, the acceleration responses of Cable C1 are taken as input of the trained model, and deflection response of point M2 is predicted accordingly. Then, the training and validation loss curves are shown in Fig. 7.

Fig. 8 compares the MGDR of point M2 predicted by the proposed method and the FEM results (the three operating cases are not included in the training set). The predicted results are in good agreement with the FEM, and the maximum relative error is only 4.7%. The maximum deflection predicted by the proposed method for each case occurs at t = 9.6 s, t = 38 s and t = 6.7 s, with values of 44.3 mm, 42 mm and 46.2 mm, respectively. While the maximum deflection obtained b FEM also occurs at the same time, with values of 44 mm, 41 mm and 45.8 mm respectively, thus the relative errors of the maximum deflection are 0.6%, 2.4% and 0.6%, respectively. And the

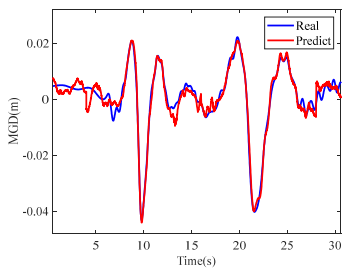

(a) Results of the first test group

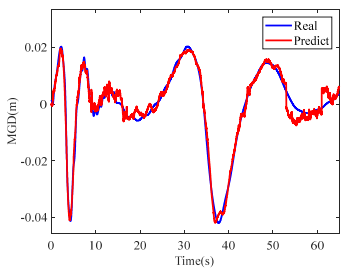

(b) Results of the second test group

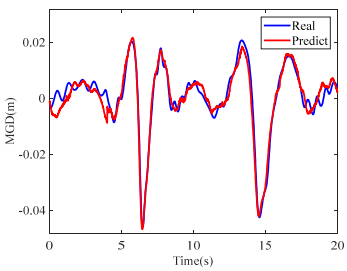

(c) Results of the third test group

Fig. 8 The predicted results of the numerical cable-stayed bridge induced by single moving vehicle

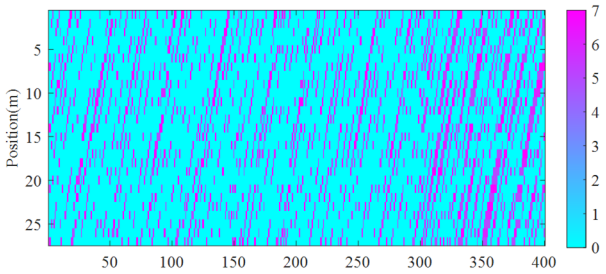

Fig. 9 The position and mass ratio of vehicles in the random traffic flow

RMSE of each case is 0.0224, 0.0222 and 0.0281, respectively. The model output results fluctuate around zero due to the fact that loss function tries to reduce the effect of the data near the zero and enhance peak fitting.

5.2 Monitoring of MGDR induced by random traffic load

As single vehicle cannot simulate the real vehicle load in operation, the meta cellular automaton (Chen and Wu 2011) is used to simulate the random traffic flow. The simulated random traffic load is substituted into the BFEM to calculated the dynamic response. And the CFEM is used to calculate CAR. Fig. 9 shows the typic random traffic load, and Fig. 10 displays the corresponding CAR and MGDR responses.

The first 300 s of CAR and MGDR responses induced by the random traffic load are classified as training set and the last 100 s are classified as test set. The training set is substituted into the BiLSTM neural network for training. The acceleration of C1 in test set that are substituted into the trained BiLSTM neural network to obtain the real-time deflections of point M2 and the results are plotted in Fig. 11. It can be seen that the results of the proposed method agree well with the FEM results. The maximum deflection of the predicted results (28.7 mm) and FEM results (29.6 mm) both appear at time t = 60 s, and the relative error is only 3.1%. Besides, the relative errors between the monitoring results and FEM results when the deflection over 15 mm are all less than 7.8%. And the RMSE of the result is 3.9795.

5.3 Measurement noise effect

In real operation environment, measurement noise is unavoidable. To evaluate the measurement noise effect on the effectiveness of the proposed method, measurement noise is intruded in the CAR response of test set in Section 5.2 according to the signal-to-noise ratios of 10 db, 20 db and 30 db, respectively. Then the noise-polluted responses are substituted into the trained model in Section 5.2, and the corresponding results are shown in Fig. 12. The results indicate that the output results of the trained model are almost unaffected when the signal-to-noise ratio reaches 20 dB, while they deviate but with the same trends when the signal-to-noise ratio is 5 dB. The predicted results with the signal-to-noise ratio of 5 dB, 10 dB, and 20 dB as input are 13.9 mm, 14.8 mm, and 15.2 mm at t = 60 s, and the corresponding relative errors are 9.1%, 3.2%, and 0.6%, respectively. The proposed model is proved to be robust and effective for application.

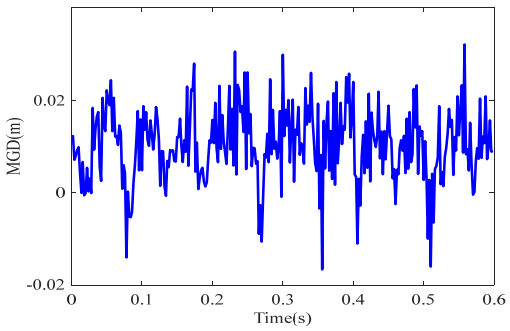

(a) The deflection of point M2 in train set

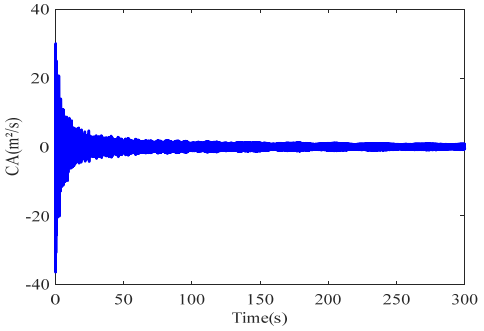

(b) The acceleration of C1 in train set

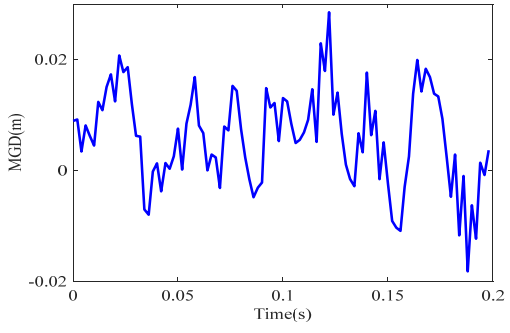

(c) The deflection of point M2 in test set

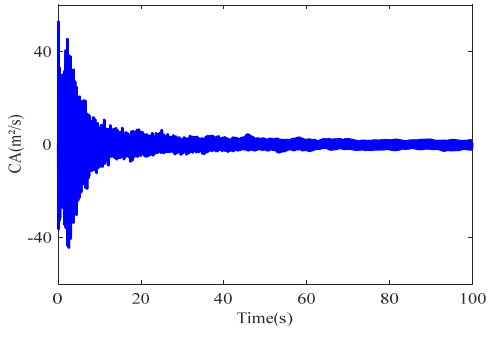

(d) The acceleration of C1 in test set

Fig. 10 The dataset of the numerical cable-stayed bridge induced by induced by random traffic load

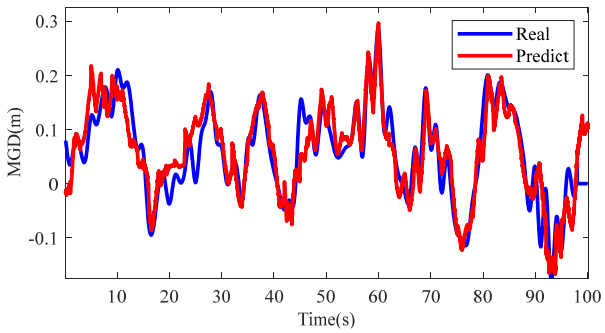

Fig. 11 The predicted results of the numerical cable-stayed bridge induced by random traffic load

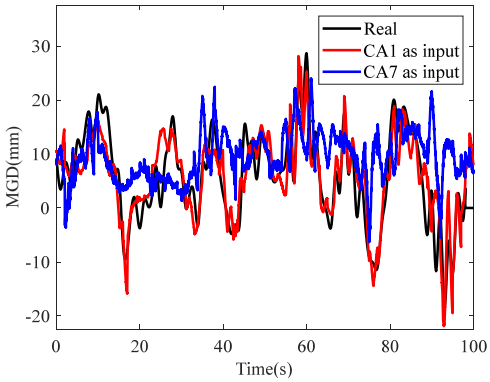

Fig. 13 Effect of the length of the measuring cable

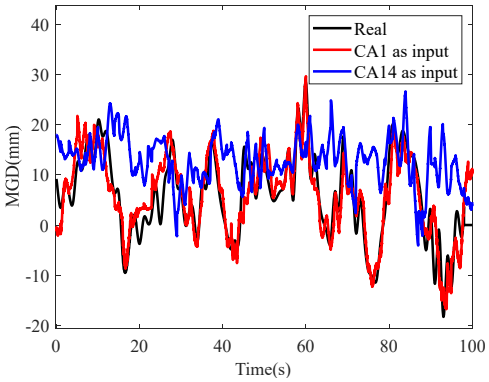

Fig. 14 Effect of the distance between the measuring cable and the target point

5.4 Sensor arrangement effect

It is promising to use a limited number of sensors for a real bridge health monitoring system considering economic cost and maintenance workload. This subsection aims to investigate the effect of sensor arrangement on the effectiveness of the proposed method.

(1) Effect of the measuring cable length. The MGDR of point M2 is predicted with C1 (Length of 32 m) and C7 (Length of 6 m) at the same time, and the results are shown in Fig. 13. Noted that the distance from point M2 to C1 and C7 anchorage are both 12 m. When the CAR of C7 is taken as input for network training, significant errors can be found in the predicted result. The RMSE of the CA1 and CA7 as the input is 3.9795, 9.078 respectively. On the contrary, when the CAR of C1 is taken as input for network training, the final result match the real deflection well. It can be concluded that taking the acceleration of long cables as

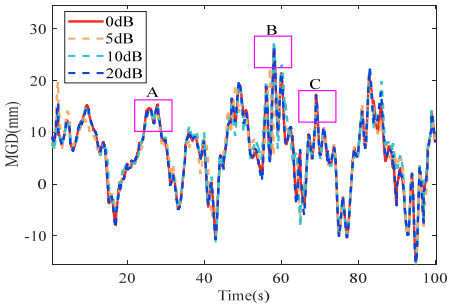

(a) Original

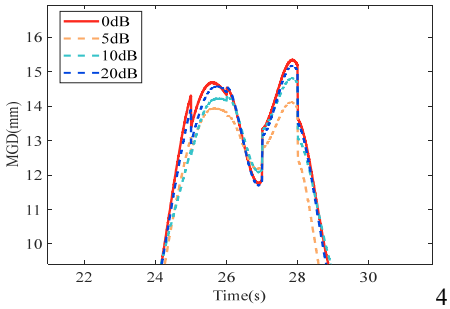

(b) Scale of A

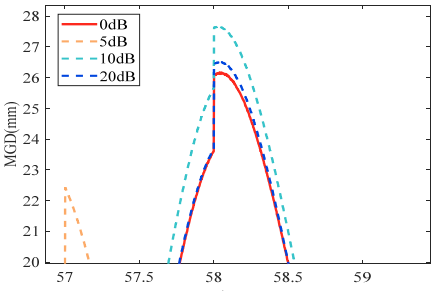

(c) Scale of B

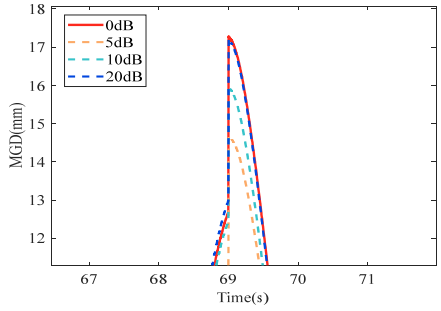

(d) Scale of C

Fig. 12 Measurement noise effect on the proposed method

model input is better than short cables.

(2) Effect of the distance between the measuring cable and the target point. The point M4 is predicted by C1 (Length of 32 m) and C14 (Length of 32 m) at the same time, and the results are shown in Fig. 14. Noted that the distance from point M2 to the anchorage points of C1 and C14 are 14 m and 42 m, respectively. The predicted result with the CAR of C1 as input for network training is much better than that of CAR of C14. The RMSE of the CA1 and CA14 as the input is 3.9795, 11.3993 respectively. The maximum deflection is 28.6 mm at t = 60 s, and the corresponding relative error is 2.8%, which indicates that taking acceleration of cables closer to the monitoring point as model input led to better results.

6. Field test

The proposed method is applied to a real bridge to verify its effectiveness and superiority. Fig. 15 shows the G15 (Shenhai Expressway) Guan-he Cable-stayed Bridge in Jiangsu Province, China. The main parameters of the bridge are listed in Table 2. The cables are numbered LS1 ~ LS52 from left to right (Fig. 16). And Fig. 16 shows the CAR monitoring points at the LS27 and deflection monitoring points (Point M1-M3) on the cable-stayed bridge. Acceleration sensors are arranged on the cable to obtain CAR (Fig. 16). Luminous sheets are placed under the main girders and a non-contact multi-point dynamic displacement detection system is used to obtain MGDR (Fig. 16). Fig. 17 presents the instruments for acquiring CAR and MGDR.

Due to the limitation of monitoring conditions, the data monitored from 3:00 pm to 3:40 pm on September 1, 2022 are selected for comparative analysis. During this period, the traffic flow is more complex and the monitoring data are more complicated, which is more representative to examine the effectiveness of the proposed method. However, the temperature effect is neglected, since the temperature variation is small in such a short time. The relationship model to monitor MGDR through CAR based on BiLSTM neural network is established following the steps described in Section 2.4. The acceleration sensor was installed on the cable LS27, and Fig. 18 shows the measured acceleration response. While the non-contact multi-point dynamic displacement detection system is used to monitor the MGDR of the position of the luminous lights installed at the mid-span (Fig. 19). The first 700 s and last 1100 s of monitored CAR and MGDR are taken as test set and train set, respectively (Figs. 18 and 19). The deflection at the t = 0 s is set as the initial deflection, and the monitored deflections are the relative deflections with respect to the initial deflection.

Firstly, the CAR and MGDR in the training set are used as input and output to the model based on BiLSTM neural network for training. Then the CAR in test set is substituted into the trained model to predict the MGDR. Finally, the predicted MGDR is compared with the results obtained

Fig. 15 Guan-he Bridge

Fig. 17 Guan-he Bridge

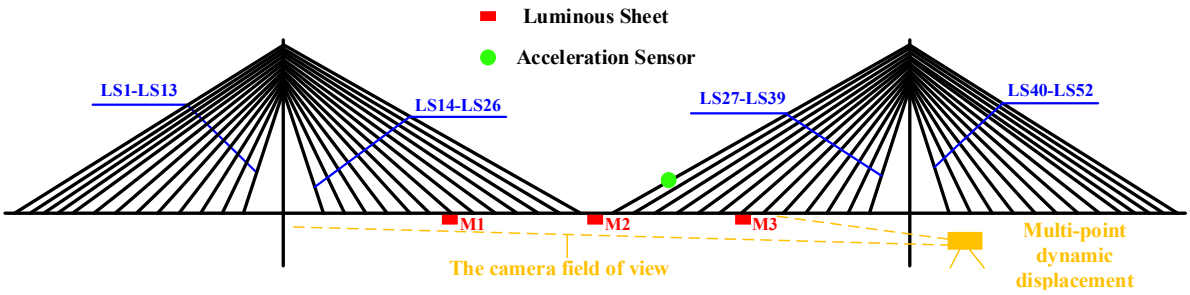

Fig. 16 The measurement layout of the Guan-he Bridge

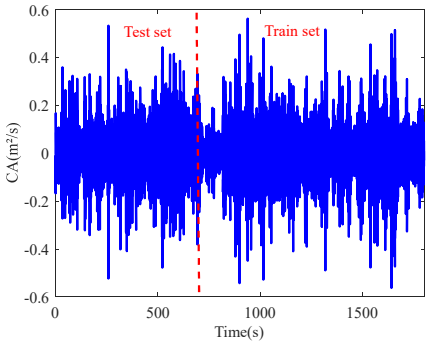

Fig. 18 The CAR of LS27 of Guan-he Bridge

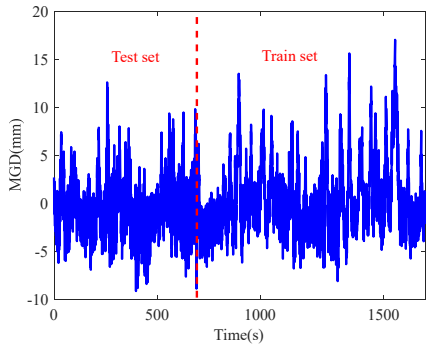

Fig. 19 The MGDR at mid-span of Guan-he Bridge

by the non-contact multi-point dynamic displacement detection system (Fig. 20). Although the amount of dataset is small, the model based on BiLSTM neural network achieves high prediction accuracy. Though minor differences can be found between the dynamic deflections obtained by the multi-point dynamic displacement detection system and the proposed method, the changing trends are basically the same.

The peak point of the deflection curve represents the time when the vehicle passing the bridge midspan. The maximum deflection measured by the non-contact multi-point dynamic displacement detection system at the time t = 255 s is 12.6 mm and the predicted deflection is 12.3 mm, with a relative error of 2.4%. And the RMSE of the result is 1.5782. However, the monitoring results are shifted around t = 650 s, which may be due to the poor fitting ability of the model near zero caused by the weighting factor of the loss function, and the peak point of the monitoring results at t = 630 s shifts, the reason may be that the similar distributions are not included in the small train set. The results of the field test proves that the proposed method provides a cost-effective and convenient way for real-time deflection monitoring of long-span cable-stayed bridges.

6. Conclusions

This paper presented a dynamic deflection monitoring method for cable-stayed bridges based on the BiLSTM neural network. Firstly, the CAR of one cable and MGDR at the target point were measured through sensors simultaneously. Then a data-driven relational model was established by the measured CAR and MGDR data and updated by the Adam optimizer. Subsequently, the hyperparameters of the relational model were adjusted according to its performance on the test set. Finally, the output of relational model was used to reconstruct real time

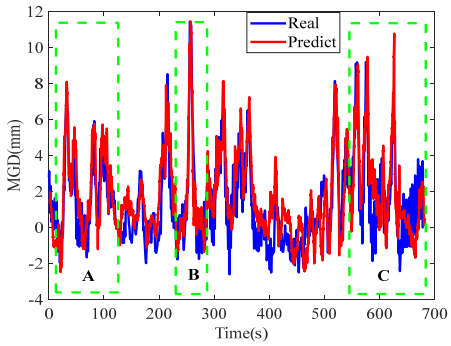

(a) Original

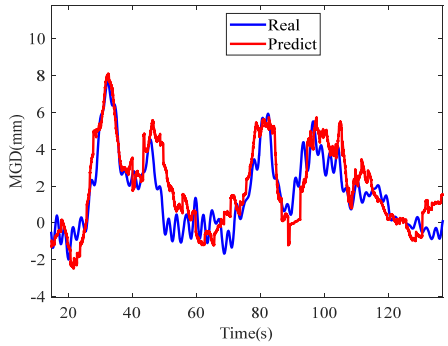

(b) Scale of A

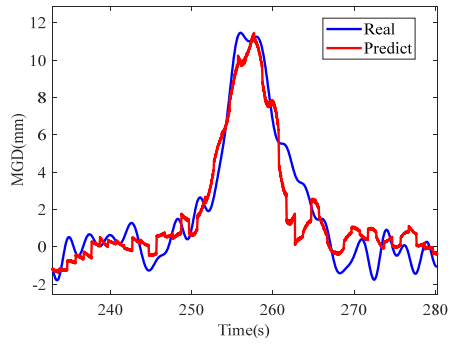

(c) Scale of B

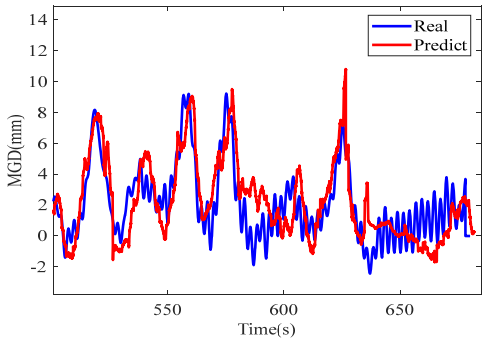

(d) Scale of C

Fig. 20 The results of the field test

MGDR. The feasibility and effectiveness of the proposed method were verified by numerical examples and field test. The results of the numerical examples indicated that the relative error of the deflection predicted by the proposed method was within 8%, and the RMSE of results are less than 4, and taking the acceleration of the long cables and cables closer to the monitoring point as model input would lead to better results. The proposed method was further used to monitor the main girder deflection of the Guan-he Bridge. Minor differences could be found between the dynamic deflections obtained by multi-point dynamic displacement detection system and the proposed method, but the changing trends were basically the same, the relative error of the result at the maximum peak point is 2.4%, and the RMSE of result is 1.5782. Since the acceleration responses of the cables were already automatically monitored in the health monitoring system without additional equipment, the proposed method was a cost-effective and convenient way for real-time deflection monitoring of long-span cable-stayed bridges.

Acknowledgments

The paper is supported by National Natural Science Foundation of China (52378298), and Natural Science Fund for Distinguished Young Scholars of Anhui Province (2208085J20).

References

ANSYS (2014), ANSYS Multiphysics, Release 14.5, ANSYS Inc.; Canonsburg, PA, USA.

Avsar, Ö., Akca, M.D. and Altan, M.O. (2014), "Photogrammetric deformation monitoring of the second Bosphorus Bridge in Istanbul", *Int. Soc. Photogram. Remote Sensing*, **XL-5**, 23-25. https://dx.doi.org/10.5194/ isprsarchives-XL-5-71-2014

Beshr, E.W. and Kaloop, M.R. (2013), "Monitoring bridge deformation using auto-correlation adjustment technique for total station observations", *Positioning.*, **4**, 1-7. https:// doi.org/ 10.4236/pos.2013.41001

Chen, S.R. and Wu, J. (2011), "Modeling stochastic live load for long-span bridge based on microscopic traffic flow simulation", *Comput. Struct.*, **89**(9-10), 813-824. https://doi.org/10.1016/j.compstruc.2010.12.017

Fan, G., Li, J. and Hao, H. (2019), "Lost data recovery for structural health monitoring based on convolution neural networks", *Struct. Control. Hlth.*, **26**(10), e2433. https: //doi.org/10.1002/stc.2433

Fan, G., Li, J. and Hao, H. (2020), "Vibration signal denoising for structural health monitoring by residual convolution neural networks", *Measurement*, **157**, 107651. https://doi.org/ 10.1016/j.measurement.2020.107651

Fan, G., Li, J., Hao, H. and Xin, Y. (2021), "Data driven structural dynamic response reconstruction using segment based generative adversarial networks", *Eng. Struct.*, **234**, 111970. https://doi.org/ 10.1016/j.engstruct.2021.111970

Gaxiola-Camacho, J.R., Bennett, R., Guzman-Acevedo, G.M. and Gaxiola-Camacho, I.E. (2017), "Structural evaluation of dynamic and semi-static displacements of the Juarez Bridge using GPS technology", *Measurement*, **110**, 146-153. https:// doi.org/10.1016/j.measurement.2017.06.026

He, W.Y., Liu, P., Cheng, H.C., Li, Z.B. and Bu, J.Q. (2022), "Displacement reconstruction of beams subjected to moving load using data fusion of acceleration and strain response", *Eng. Struct.*, **268**, 114693. https://doi.org/10.1016/j.engstruct.2022. 114693

Huang, Q., Crosetto, M., Monserrat, O. and Crippa, B. (2017), "Displacement monitoring and modelling of a high-speed railway bridge using C-band Sentinel-1 data", IS*PRS. J. Photogramm.*, **68**(1), 138-149. https://doi.org/10.1016/j. isprsjprs.2017.03.016

Huang, Y., Wang, Y., Fu, J., Liu, A. and Gao, W. (2018), "Measurement of the real-time deflection of cable-stayed bridge based on cable tension variations", *Measurement*, **119**, 218-228. https://doi.org/10.1016/j.measurement.2018.01.070

Irving, H.M. (1981), *Cable Structures*, MIT press, Cambridge, MA, USA.

Khuc, T. and Catbas, F.N. (2017), "Completely contactless structural health monitoring of real-life structures using cameras and computer vision", *Struct. Control. Hlth.*, **24**(1), e1852. https://doi.org/10.1002/stc.1852

Kingma, D.P. and Ba, J. (2021), "Adam: A method for stochastic optimization", arXiv preprint, 1412, 6980. https://doi.org/10.48550/arXiv.1412.6980

Lee, D.H. and Koh, B.H. (2021), "An image-based deep learning network technique for structural health monitoring", *Smart Struct. Syst., Int. J.*, **28**(6), 799-810. https://dx.doi.org/10.12989/sss. 2021.28.6.799

Li, S., Wang, X., Liu, H., Zhuo, Y., Su, W. and Di, H. (2020), "Dynamic deflection monitoring of high-speed railway bridges with the optimal inclinometer sensor placement", *Smart Struct. Syst., Int. J.*, **26**(5), 591-603. https://dx.doi.org/10.12989/sss.2020.26.5. 591

Ma, T.W., Bell, M., Xu, N.S. and Lu, W. (2014), "Recovering structural displacements and velocities from acceleration measurements", *Smart Struct. Syst., Int. J.*, **14**(2), 191-207. https://dx.doi.org/10.12989/sss.2014.14.2.191

Nguyen, V.H., Schommer, S., Maas, S. and Zürbes, A. (2016), "Static load testing with temperature compensation for structural health monitoring of bridges", *Eng. Struct.*, **127**, 700-718. https:// doi.org/10.1016/j.engstruct.2016.09.018

Ni, F.T., Zhang, J. and Chen, Z.Q. (2019), "Pixel-level crack delineation in images with convolutional feature fusion", *Struct. Control. Hlth.*, **26**(1), e2286. https://doi.org/10.1002/stc.2286

Ni, F.T., Zhang, J. and Noori, M.N. (2020), "Deep learning for data anomaly detection and data compression of a long-span suspension bridge", *Comput-Aided. Civil Inf.*, **35**(7), 685-700. https:// doi.org/10.1111/mice.12528

Park, K.T., Kim, S.H., Park, H.S. and Lee, K.W. (2005), "The determination of bridge displacement using measured acceleration", *Eng. Struct.*, **27**(3), 371-378. https://doi.org/ 10.1016/j.engstruct.2004.10.013

Paszke, A., Gross, S., Massa, F., Lerer, A., Bradbury, J., Chanan, G., Killeen, T., Lin, Z., Gimelshein, N., Antiga, L. and Desmaison, A. (2019), "Pytorch: An imperative style, high-performance deep learning library", arXiv preprint, 1912, 01713. https://doi.org/10.48550/arXiv.1412. 6980

Pendharkar, U., Chaudhary, S. and Nagpal, A.K. (2010), "Neural networks for inelastic mid-span deflections in continuous composite beams", *Struct. Eng. Mech., Int. J.*, **20**(2), 219-229. https://dx.doi.org/10.12989/sem.2010.36.2.165

Shin, J.U., Jeon, H., Choi, S., Kim, Y. and Myung, H. (2016), "Laser pose calibration of ViSP for precise 6-DOF structural displacement monitoring", *Smart Struct. Syst., Int. J.*, **18**(4), 801-818. https://dx.doi.org/10.12989/sss.2014.14.2.191

Stiros, S.C. (2021), "GNSS (GPS) Monitoring of dynamic deflections of bridges: Structural constraints and metrological limitations", *Infrastructures*, **6**(2), 23. https://doi.org/10.3390/ infrastructures6020023

Tadesse, Z., Patel, K.A., Chaudhary, S. and Nagpal, A.K. (2012), "Neural networks for prediction of deflection in composite bridges", *J. Constr. Steel Res.*, **68**(1), 138-149. https:// doi.org/10.1016/j.jcsr.2011.08.003

Tian, Y., Xu, Y., Zhang, D. and Li, H. (2021), "Relationship modeling between vehicle-induced girder vertical deflection and cable tension by BiLSTM using field monitoring data of a cable-stayed bridge", *Struct. Control. Hlth.*, **28**(2), e2667. https: //doi.org/10.1002/stc.2667

Wang, X., Li, Z., Zhuo, Y., Di, H., Wei, J., Li, Y. and Li, S. (2021), "Indirect displacement monitoring of high-speed railway box girders consider bending and torsion coupling effects", *Smart Struct. Syst., Int. J.*, **28**(6), 827-838. https://dx.doi.org/10.12989/sss. 2021.28.6.827.

Xu, Y., Brownjohn, J. and Kong, D. (2018), "A non-contact vision-based system for multipoint displacement monitoring in a cable-stayed footbridge", *Struct. Control. Hlth.*, **25**(5), e2155. https://doi.org/10.1002/stc.2155

Yi, T.H., Ye, X.W., Li, H.N. and Guo, Q. (2017), "Outlier detection of GPS monitoring data using relational analysis and negative selection algorithm", *Smart Struct. Syst., Int. J.*, **20**(2), 219-229. https://dx.doi.org/10.12989/sss.2017.20.2.219

Yu, S., Xu, Z., Su, Z. and Zhang, J. (2021), "Two flexible vision-based methods for remote deflection monitoring of a long-span bridge", *Measurement.*, **181**, 109658. https://doi.org/10.1016/j. measurement.2021.109658

Zhou, J., Sun, Z., Wei, B., Zhang, L. and Zeng, P. (2021), "Deflection-based multilevel structural condition assessment of long-span prestressed concrete girder bridges using a connected pipe system", *Measurement*, **169**, 108352. https://doi.org/ 10.1016/j.measurement.2020.108352

Zhuge, S., Xu, X., Zhong, L., Gan, S., Lin, B., Yang, X. and Zhang, X. (2022), "Noncontact deflection measurement for bridge through a multi-UAVs system", *Comput-Aided. Civil Inf.*, **37**(6), 746-761. https://doi.org/10.1111/mice.12771